Available online at www.sciencedirect.com
ScienceDirect
Composite Structures 79 (2007) 581–589
COMPOSITE STRUCTURES
www.elsevier.com/locate/compstruct

The effect of Stone–Wales defect on the tensile behavior and fracture of single-walled carbon nanotubes

K.I. Tserpes [a,*], P. Papanikos [b]

[a] Laboratory of Structural Mechanics, Department of Rural and Surveying Engineering, National Technical University of Athens, Zografou Campus, 9 Iroon Polytechniou St., 15780 Athens, Greece
[b] Department of Product and Systems Design Engineering, University of the Aegean, Ermoupolis, Syros 84100, Greece

Available online 18 April 2006

Abstract

The effectiveness of carbon nanotubes as reinforcements in the next generation of composites is designated by their mechanical behavior as standalone units. One of the most commonly present topological defects, whose effect on the mechanical behavior of carbon nanotubes needs to be clarified, is the Stone–Wales (SW) defect. In this paper, the effect of SW defect on the tensile behavior and fracture of armchair, zigzag and chiral single-walled carbon nanotubes (SWCNTs) was studied using an atomistic-based progressive fracture model. The model uses the finite element method for analyzing the structure of SWCNTs and the modified Morse interatomic potential for describing the nonlinear force-field of the C–C bonds. In all cases examined, the SW defect serves as nucleation site for fracture. Its effect on the tensile behavior of the SWCNTs depends solely on nanotube chirality. In armchair SWCNTs, contrary to zigzag ones, a significant reduction in failure stress and failure strain was predicted; ranging from 18% to 25% and from 30% to 41%, respectively. In chiral SWCNTs, the effect of the defect is between those of the armchair and zigzag SWCNTs, depending on chiral angle. The stiffness of the nanotubes was not affected. The nanotube size was found to play a minimal role in the tensile behavior of SW-defected SWCNTs; only in cases of very small nanotube diameters, where the fraction of defect area to the nanotube area is high, was a larger decrease in the failure stress predicted.

Keywords: Carbon nanotubes; Finite element analysis; Interatomic potential; Progressive fracture analysis; Stone–Wales defect

1. Introduction

Due to their extraordinary mechanical properties, carbon nanotubes (CNTs) are being considered as the ideal reinforcing material for the next generation of composites. In this role, CNTs' performance is designated by their mechanical behavior as stand alone units. So far, in the majority of studies, CNTs have been treated as defect-free materials. However, experimental observations [1] have revealed that topological defects, such as the Stone–Wales (SW) defect, and vacancy defects, are commonly present. The presence of defects in CNTs is consolidated by the recent findings of Mielke et al. [2] who predicted that the presence of vacancy defects significantly reduces the failure stress and failure strain of CNTs providing an explanation for the extant theoretical–experimental discrepancies.

The SW defect is the most important defective structure in CNTs. Investigations have shown that besides the effect that may have on the mechanical behavior of CNTs, SW defect also affects their electronic, magnetic and hybridization characteristics. Because of its multiple effect, the SW defect demonstrates several utilities. For example, the transition in the Y junction, contemplated in CNT based molecular electronics, is achieved through the incorporation of many SW defects either by design or otherwise [3]. Similarly, a transition of nanotubes from one diameter to another can be achieved by locating a few SW defects strategically in the transition region. In addition, when nanotubes are used as fibers in nanocomposites, interfacial

* Corresponding author. Tel.: +30 210 9886743; fax: +30 210 8254177.
E-mail address: kit2005@otenet.gr (K.I. Tserpes).

0263-8223/$ - see front matter © 2006 Elsevier Ltd. All rights reserved.
doi:10.1016/j.compstruct.2006.02.020

bonding may preferably occur in these defected regions based on energy considerations. Another area in which the SW defect offers some advantage is the effective storage of hydrogen for possible use in fuel cells. In this case, the propensity for hydrogen penetrating the defected region and entering the tube is higher than in the regular regions.

In any case, before taking advantage of any of the utilities of SW defect, such as those described above, its effect on the mechanical behavior of CNTs needs to be fully clarified. Since experiments at this length scale are still under development, theoretical modeling serves as the only available tool to achieve this goal. To date, several atomistic modeling studies have considered the presence of SW defect in CNTs, but its effect on the mechanical behavior of the nanotubes has not been studied. In the present paper, the effect of SW defect on the tensile behavior and fracture of SWCNTs was studied using an atomistic-based progressive fracture model.

2. The Stone–Wales defect in CNTs: a short overview

Defects in CNTs, either introduced during the synthesis process or stress induced ones, may be divided into three categories:

(i) topological defects, such as the SW transformation [4],
(ii) rehybridization defects, which refer to the change from sp^2 to sp^3 of a C–C bond due to highly localized deformation, and
(iii) incomplete bonding and other defects, such as impurity attachments, substitutions and vacancies.

The SW defect was originally presented as the 'Stone–Wales transformation' [4] and referred to the rotation of a bond shared by two adjacent hexagons in icosahedral C_{60}, which results in an unfavorable conformation having two adjacent pentagons. Thus, the usage of the term in the CNT literature is a generalization of the original usage. Briefly, the SW defect in CNTs may be described as the 90° rotation of a bond that transforms 4 hexagons into 2 pentagons and 2 heptagons. A schematic of the defect formation in the hexagonal (armchair) lattice is shown in Fig. 1.

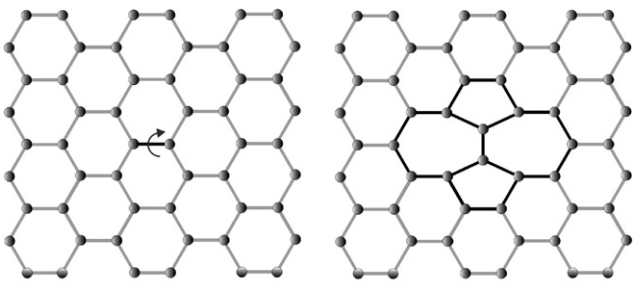

Fig. 1. Schematic of the SW formation in the hexagonal lattice of CNTs: (a) pristine lattice and (b) SW-defected lattice.

Mechanics of SW defects and fracture of CNTs containing such defects have been studied by using atomistic modeling approaches. The following paragraphs review the results of the most important studies.

Belytschko et al. [5] were the first to include the SW defect in a simulation of CNT fracture. However, only a small part of their study was devoted to the SW defect. By using molecular dynamics (MD) simulations with the modified Morse interatomic potential they modeled a SW defect in a (12, 12) tube. They found that the SW defect gave a lower failure stress and strain than the 10% weakening of one bond at the middle of the nanotube and that the fracture is brittle. The study of SW defect was repeated with a (40, 40) tube. The obtained values for the failure stress and failure strain were similar to those of the (12, 12) tube, and the fracture was still brittle indicating a minor effect of nanotube size on the strength.

Troya et al. [6] presented quantum mechanical studies of CNT fracture by using two different semi-empirical methods. Their study was focused on the initiation and growth of fracture from a SW defect rather the influence of the defect on the mechanical behavior of CNTs. They showed that the quantum calculations do not reproduce certain details of the ring-opening fracture mechanism proposed by Yakobson [7]. Specifically, the bonds connecting the two pentagon rings were found to be stronger than bond-order empirical potentials predict, and thus, these bonds are not the weak link that permits the nucleation of SW defects. Instead, the failing bonds were observed to include those that lie within the pentagon rings. The defects considered by Troya et al. [6] were: one SW defect, an aggregation of two SW defects and an aggregation of five SW defects. It was observed that there is a reduction in failure strain of the nanotubes due to the presence of SW defects. For the (5, 5) tube containing an aggregation of five SW defects, the reduction ranges from 6.3% to 53.5% according to the method of calculation. The effect of SW defects on the failure stress of the nanotubes was not examined.

Chandra et al. [8] adapted three different stress measures at atomic scales and introduced strain measures as energetically conjugate quantities to study the local properties of SW defects in SWCNTs under axial tension. The study involved the consideration of one SW defect in various mostly zigzag SWCNTs with different diameters. In the (9, 0) tube, two types of SW defects, one symmetric and one asymmetric, were considered. It was found that the stiffness of defects reduces by about 30–50% and is dependent on a number of factors such as the chirality, the diameter of the nanotubes and the loading conditions. Similar to Troya et al. [6], Chandra et al. [8] did not examine the effect of SW defects on the failure stress of the nanotubes. Moreover, Chandra et al. [8] did not consider fracture of CNTs.

Mielke et al. [2] used quantum mechanical calculations using density functional theory and semi-empirical methods, and MD calculations with a Tersoff–Brenner potential to explore the role of vacancy defects in the fracture of

CNTs under axial tension. Among the defects considered was a single SW defect. All methods predicted a clear reduction of both fracture stress and strain due to the presence of the SW defect.

3. Progressive fracture modeling

Atomistic-based continuum mechanics approaches developed for CNTs are a combination of a structural analysis method, which is used to analyze the structure of CNTs, with an interatomic potential, which describes the behavior of the C–C bonds. In Ref. [9], Tserpes and Papanikos developed a finite element (FE) model for SWCNTs, which assumes a linear behavior of C–C bonds. Its applicability is, therefore, limited to cases where very small nanotube deformation takes place. To overcome this restriction, a progressive fracture model (PFM) able to simulate the behavior of SWCNTs under various mechanical loading conditions was proposed [10]. The PFM uses the FE model to analyze the structure of CNTs and an interatomic potential to describe the nonlinear behavior of the C–C bonds. In the following, the PFM is briefly described.

3.1. Simulation of the nonlinear behavior of the C–C bonds

There are two types of interatomic potentials: pairwise and many-body. The major difference between them lies in the consideration of non-bonded interactions by many-body potentials. In general, pairwise potentials are in disadvantage over many-body ones especially in cases where the molecular systems sustain large deformations. In such cases, large deviations of the atoms from the equilibrium take place imposing multiple large non-bonded interactions with their nearest neighbors, which must be taken into account. However, for restricting the pair potential to nearest neighbors, many-body potentials introduce a cut-off function, which has found to cause strange features in the resulting force–strain curve. Belytschko et al. [5] found that in the Brenner many-body potential [11] the cut-off function causes a dramatic increase in the interatomic force (like a camelback) at the inflection point, which affects fracture behavior of the bond, and consequently of the nanotube, even when it is shifted to 100% strain.

In the PFM, the pairwise modified Morse potential was used. This decision was strongly influenced by the simplicity of the specific potential over many-body potentials. To date, the modified Morse potential has been adequately applied in a number of cases where there are large deviations from equilibrium due to the presence of large strains. Belytschko et al. [5] and Tserpes et al. [10] applied the potential for simulating fracture of CNTs subjected to axial tension, Xiao et al. [12] for predicting the mechanical properties of CNTs and Sun and Zhao [13] for predicting stiffness and strength of SWCNTs.

The modified Morse potential is not appropriate for describing the behavior of CNT when bonds are broken, since it does not allow for reconfiguration of bonds. However, as shown by Belytschko et al. [5], the fracture strength of CNTs depends primarily on the inflection point of the interatomic energy and is almost independent of the dissociation energy. Therefore, since the inflection strain occurs substantially before the strain associated with bond breaking, where the formation of other bonds is expected, the independence of fracture strength to the dissociation energy provides some confidence that the modified Morse potential can give a correct picture of nanotube fracture in cases of moderate temperatures (0–500 K). Such is the current case where the specific potential was used to study the effect of SW defect on the tensile behavior and fracture of SWCNTs. At low temperatures, SW defects are expected to result in fracture, while at high temperatures to plastic response.

According to the modified Morse potential, the potential energy of the nanotube system is expressed as

$$E = E_{\text{stretch}} + E_{\text{angle}}, \tag{1}$$

$$E_{\text{stretch}} = D_{\text{e}}\left\{1 - [\text{e}^{-\beta(r-r_0)}]^2 - 1\right\}, \tag{2}$$

$$E_{\text{angle}} = \tfrac{1}{2}k_\theta(\theta-\theta_0)^2\left[1 + k_{\text{sextic}}(\theta-\theta_0)^4\right], \tag{3}$$

where E_{stretch} is the bond energy due to bond stretching and E_{angle} the bond energy due to bond angle-bending, r is the current bond length and θ is the current angle of the adjacent bond. The parameters of the potential are [5]:

$$r_0 = 1.421\times10^{-10}\ \text{m},\quad D_{\text{e}} = 6.03105\times10^{-19}\ \text{N m},$$
$$\beta = 2.625\times10^{10}\ \text{m}^{-1},\quad \theta_0 = 2.094\ \text{rad},$$
$$k_\theta = 0.9\times10^{-18}\ \text{N m/rad}^2,\quad k_{\text{sextic}} = 0.754\ \text{rad}^{-4}.$$

This is the usual Morse potential except that the bond angle-bending energy has been added and the parameters have been slightly modified by Belytschko et al. [5] so that it corresponds with the Brenner potential [11] for strains below 10%. As bond stretching dominates nanotube fracture and the effect of angle-bending potential is very small, only the bond stretching potential is considered.

By differentiating Eq. (2), the stretching force of atomic bonds is obtained in the molecular force-field as

$$F = 2\beta D_{\text{e}}\left(1 - \text{e}^{\beta(r-r_0)}\right)\text{e}^{-\beta(r-r_0)}. \tag{4}$$

Fig. 2 plots the relationship between force F and bond strain ε for the C–C bonds. The strain of the bond is defined by $\varepsilon = (r - r_0)/r_0$. As may be seen, the force–strain relation is highly nonlinear at the attraction region especially at large strains. The inflection point (peak force) occurs at 19% strain. The repulsive force ($\varepsilon < 0$) increases rapidly as the bond length shortens from the equilibrium length with less nonlinearity than the attractive force.

3.2. Algorithm of the model

For modeling the C–C bonds, the 3D elastic ANSYS BEAM4 element was used. The nonlinear behavior of the

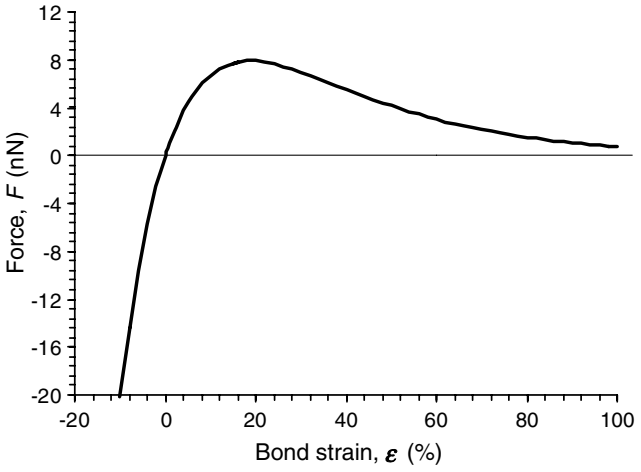

Fig. 2. The force–strain curve of the modified Morse potential.

C–C bonds, as described by the interatomic potential, was assigned to the beam elements using the stepwise procedure of progressive fracture modeling, which is briefly described in the following lines. Initially, the stiffness of the beam elements is evaluated from the initial slope of the force–strain curve of the modified Morse potential (Fig. 2) using the element's cross sectional area A. The initial stiffness is 1.16 TPa. The nanotube is loaded by an incremental displacement at one end with the other end fixed. At each load step, the stiffness of each element is set equal to $F/A\varepsilon$, where ε is the axial strain of the element as evaluated from the FE model and F is the interatomic force calculated using Eq. (4) given the ε. The next displacement increment is then applied to the nanotube and this iterative procedure goes on until catastrophic failure of the nanotube takes place.

The accuracy of the progressive fracture modeling procedure depends on the number of load steps chosen. In order to maximize the accuracy of computational results, in each case, the displacement increment was chosen from convergence tests in which the convergence criterion was set equal to 2% of the failure stress. Thereby, if between two sequential displacement increments a difference smaller than the 2% was achieved in the computed failure stress, the larger displacement increment was finally adopted for the analysis.

4. Formation of SW defect

Beyond a critical value of tension, a CNT releases its excess tension via formation of topological defects. Such a defect is the SW defect. In the case of armchair nanotubes under axial tension, where a transverse tension takes place (the applied load is perpendicular to the C–C bonds), the excess strain is released via the 90° rotation of the perpendicular bond (see Fig. 1). In contrast, in the case of zigzag nanotubes under axial tension, the C–C bonds are parallel to the applied load, which is already the minimum energy configuration for the strained bonds. Therefore, the formation of SW defect in zigzag nanotubes is limited to the rotation of the bonds oriented 120° with respect to the tube axis.

It has been established from simulations that in armchair SWCNTs, SW defects are formed at around 5–6% applied tensile strain [14–16] and in zigzag SWCNTs at around 12% [16]. For the chiral SWCNTs, no relative information has been reported. In this study, as a strain barrier for the formation of the SW defect the value of 5% was adopted for the armchair and chiral SWCNTs, and the value of 12% for the zigzag SWCNTs.

The transformation of 4 hexagons to 2 pentagons and 2 heptagons leads to the elongation of the structure along the axis connecting the pentagons and shrinkage along the perpendicular direction. Thus, the rotation of a bond from a predominately circumferential to a predominately axial orientation lengthens the tube but not to such a degree to change the load distribution between the bonds in the nanotube. In the current simulations, for the sake of simplicity, it was assumed that after the creation of SW defect the dimensions of the nanotubes remained unchanged.

5. Computational results

For the purpose of the current study, the zigzag (20, 0), the armchair (5, 5), (12, 12) and (18, 18) and the chiral (16, 8) nanotubes were considered. Their geometrical characteristics are depicted in Table 1. The specific SWCNTs were chosen so as to study the effect of SW defect in the presence of variable chirality and nanotube size (diameter and length). Moreover, for some of them results are available in the literature to compare with. Fig. 3 displays the FE meshes of the SW-defected SWCNTs considered. For the zigzag (20, 0) tube, two types of SW defects were considered.

5.1. Stress–strain curves

In order to apply the tensile loading in the nanotubes, the nodes of one nanotube end were fully constrained, while at the nodes of the other end an incremental axial displacement was applied. At the nodes of the loaded end, constraints of zero transverse displacement were also applied to prevent nanotube bending at high loads.

Table 1
Geometrical characteristics of the SWCNTs

SWCNT	Length, L (nm)	Diameter, D (nm)	Number of atoms
Armchair (5,5)	2.95	0.68	250
Armchair (12,12)	4.18	1.63	853
Armchair (18,18)	5.91	2.44	1200
Zigzag (20,0)	4.19	1.57	800
Chiral (16,8)	4.13	1.66	840

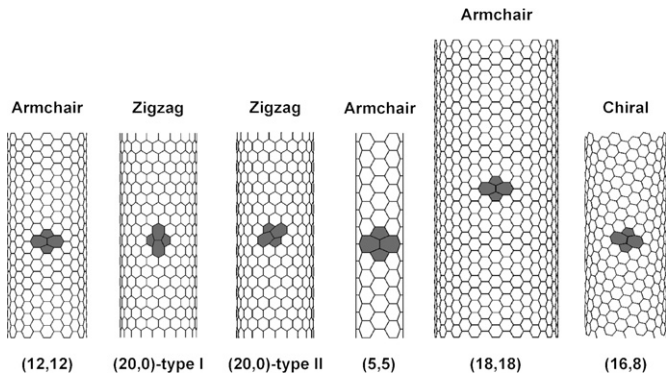

Fig. 3. FE meshes of the SW-defected SWCNTs considered. The areas enclosed to the pentagons and heptagons of the defects were colored dark gray.

Fig. 4(a)–(e) shows the predicted stress–strain curves of the SW-defected SWCNTs depicted in Fig. 3. The curves are grouped for each SWCNT. The strain of the nanotubes is given by $\varepsilon_n = (L - L_0)/L_0$, where L_0 is the initial length prior to loading and L is the current nanotube length. The stress is given by $\sigma = F_n/A_n$, F_n is the force applied in the nanotube computed by summing the longitudinal reaction forces of the constrained nodes and A_n is the cross-sectional area of the nanotube equals to πDt, where D is the diameter and t is the thickness of the nanotube (0.34 nm).

When the SW defect is formed, the bonds of the nanotube are already strained. To account for this feature, a combination of the stress–strain curve of the pristine nanotube with that of the defected nanotube was adopted. Up to the defect formation strain (5% or 12% according to nanotube chirality), the stress–strain curve of the pristine nanotube was used. For strains greater than the defect formation strain, the stress–strain curve of the defected nanotube was used. In the analysis of the defected nanotube, the first applied strain was equal to the defect formation strain. Chandra et al. [8] found that the stiffness of the nanotube area where the SW defects are located reduces by about 30–50%. According to this finding, a decrease in the nanotube stiffness should take place after the formation of the defect. However, in the present study, a marginal decrease in the nanotube stiffness was predicted only in cases where the fraction of defected area to the nanotube area was high as in the (5, 5) tube. This conclusion is supported from results of analyses performed using aggregation of SW defects in the (5, 5) tube. The results showed that with increasing number of aggregated defects, the decrease in nanotube stiffness enlarges. In any case, the decrease in stiffness remained marginal.

The SWCNTs containing SW defects predicted to exhibit a nonlinear (plastic) tensile behavior. The presence of SW defects decreases the nanotubes' failure stress and failure strain but not the stiffness. Table 2 lists the predicted failure stresses and strains. Failure stresses correspond to the peak stresses in the stress–strain curves, while failure strains to the applied strains at which the peak stresses occur. The case of the SW-defected (12, 12) tube was also considered by Belytschko et al. [5]. Using MD simulations they calculated the failure stress and failure strain to be as high as 97.5 GPa and 14.3%, respectively. These values are in good agreement with the current predicted values of 100 GPa and 12%, respectively. This agreement together with the very good agreement obtained in Ref. [10] for the vacancy defect of 1 missing atom in a (20, 0) tube verifies the PFM.

By comparing the failure stresses and strains of the pristine and defected (12, 12), (20, 0) and (16, 8) tubes, which are of the same size, it becomes evident that the reduction of these quantities depends on nanotube chirality. There is a significant reduction in the failure stress and failure strain of the armchair (12, 12) and chiral (16, 8) tubes and an insignificant one in the zigzag (20, 0) tube under the presence of both types of SW defects. This alteration is attributed to the bond rearrangement imposed by the SW defects. In the (12, 12) tube, the load carried by the four diagonal bonds (AC, BD, AE and BF bonds in Fig. 5(a)), after the formation of SW defect it is mostly carried by the longitudinal bond (GH bond in Fig. 5(b)) causing stress concentration, and consequently, early bond fracture. Fig. 6 plots the strain of the bonds joining the defect as function of nanotube strain. In the figure, the unequal distribution of strain between the bonds is clear. The GI, GJ, HK and HL bonds sustain very small strain. In the (20, 0) tube, type I SW defect does not affect the failure stress and failure strain of the nanotube because the load carried by the longitudinal bond, which is transformed to a transverse one, is balanced by the four bonds that are introduced by the side of the transverse bond. Regarding type II defect, its presence reduces the failure stress and failure strain of the (20, 0) tube by about 3% and 15%, respectively. The effect of SW defect on the tensile behavior of (16, 8) tube is similar to that of the (12, 12) tube. In general, the effect of SW defects in the chiral SWCNTs, lies between those of armchair and zigzag SWCNTs according to the chiral angle.

The role of nanotube size on the tensile behavior of SWCNTs containing SW defects can be assessed from a comparison of the results of the armchair (5, 5), (12, 12) and (18, 18) tubes, which are of different diameter and length. The comparison indicates a larger reduction in failure stress of the (5, 5) tube owing to its small diameter, which leads to high fraction of defect area to nanotube area.

5.2. Evolution of fracture

In MD simulations, bond fracture is assumed to occur when the tensile force vanishes. However, as the force–strain curve of the interatomic potential trends asymptotically to the 100% strain (see Fig. 2), the specific definition is ambiguous. In order to present fracture evolution in this section, the threshold of 80% strain was adopted.

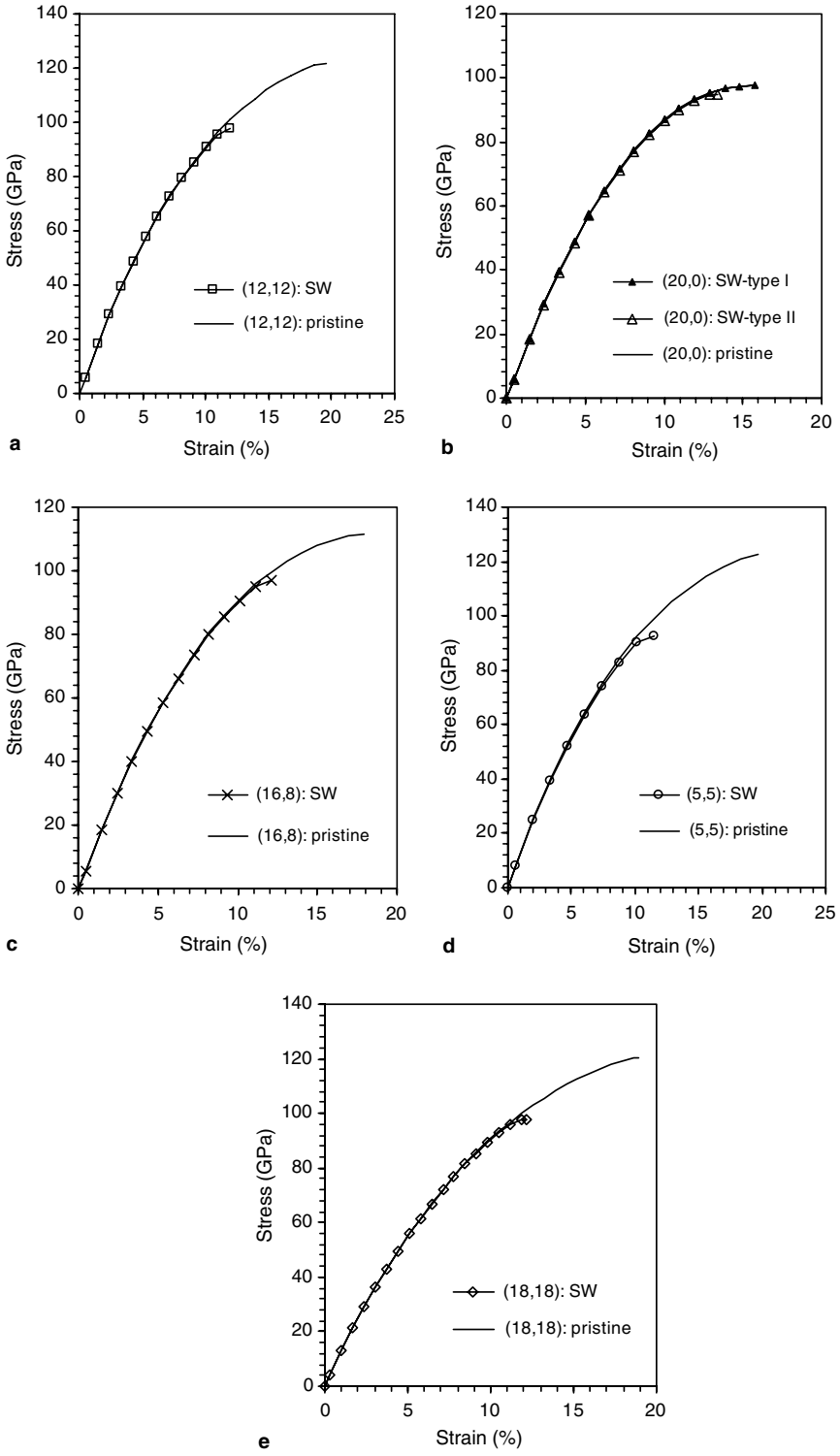

Fig. 4. Predicted stress–strain curves of the SW-defected SWCNTs. For comparison reasons, the stress–strain curves of the pristine SWCNTs were added.

Fig. 7(a) shows the prediction of fracture evolution in the (12, 12) tube containing a SW defect. Fracture initiated from the longitudinal bond connecting the two pentagons and continued in the upper diagonal bonds of the heptagons to propagate circumferentially in the row of these bonds until all bonds around circumference to have failed. The MD simulations of Belytschko et al. [5] predicted the same fracture initiation in the (12, 12) tube but different fracture propagation. They found that fracture propagated in the $\pm 45^\circ$ direction of maximum shear strain. In the present study, it was found that such fracture propagation arises when fracture is assumed to occur at the inflection

Table 2
Predicted failure stresses and strains of SW-defected SWCNTs

Nanotube	Failure stress (GPa)	Failure strain (%)
(12,12): pristine	121.86	19.61
(12,12): SW	100	11.96
(20,0): pristine	97.68	15.75
(20,0): SW-type I	97.68	15.75
(20,0): SW-type II	94.86	13.36
(16,8): pristine	114.18	17.9
(16,8): SW	96.85	12.1
(5,5): pristine	122.54	19.64
(5,5): SW	92.44	11.51
(18,18): pristine	120.63	18.96
(18,18): SW	100	12.2

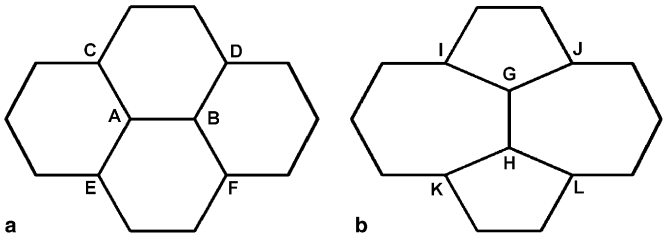

Fig. 5. Atomic configuration of the SW defect in the armchair (12,12) tube.

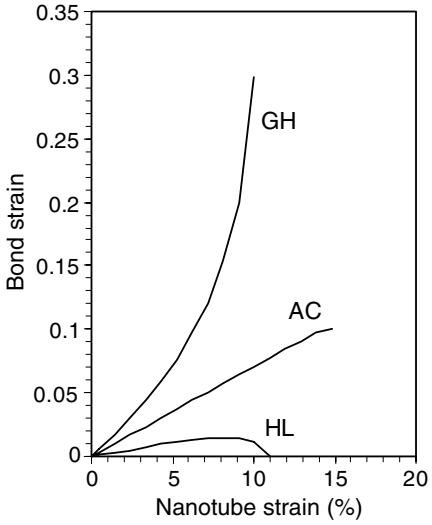

Fig. 6. Strain variation of the bonds joining the SW defect in the armchair (12,12) as function of nanotube applied strain.

point of the potential, as can be seen in Fig. 7(b). Thus, it is possible that Belytschko et al. [5] have plotted fracture using the inflection point as threshold. In any case, the current findings are more reasonable, since after the complete fracture of a bond the load that it was carrying is transferred to the neighboring bonds of the same row causing subsequent fractures.

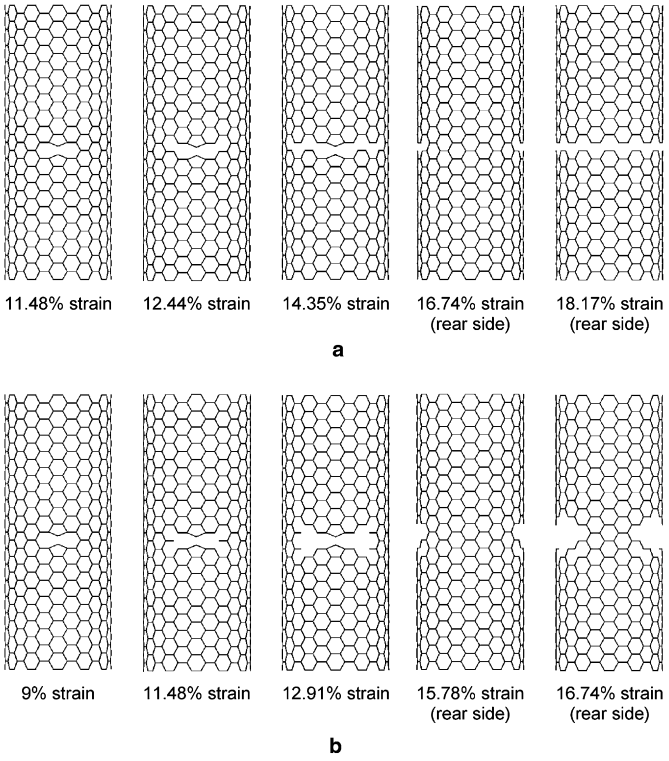

Fig. 7. Predicted fracture evolution in the armchair (12,12) tube containing a SW defect. (a) Fracture threshold at 80% strain. (b) Fracture threshold at the inflection point (19% strain).

Fig. 8(a) shows fracture evolution in the (20,0) tube containing type I SW defect. Fracture initiated from the bond of the upper heptagons and propagated circumferentially at the same row. Before final failure, some bonds at the nanotube ends were also failed due to presence of stress concentrations caused by the application of loading and boundary conditions. Fig. 8(b) shows fracture evolution in the (20,0) tube containing type II SW defect. Fracture initiated simultaneously from the bond connecting the two pentagons and two heptagons and the two bonds of the upper heptagons to propagate circumferentially in the rows of these two bonds until all bonds around circumference have failed. A similar fracture initiation and evolution was also predicted in the (16,8) tube (see Fig. 9).

In all cases, the SW defect serves as nucleation site for fracture. This stands even for the type I defect in the (20,0) tube, which does not affect nanotube tensile behavior. This is because defected regions in CNTs experience higher strains for similar values of stress compared to defect-free regions. Chandra et al. [8] have shown that the strain concentration at the defects increases with the increase of the externally applied loading and that the stiffness of SW defects reduces. The lower stiffness of the defected region is an indication of its reduced load-carrying capacity, which causes the higher localized strain concentrations that are responsible for fracture.

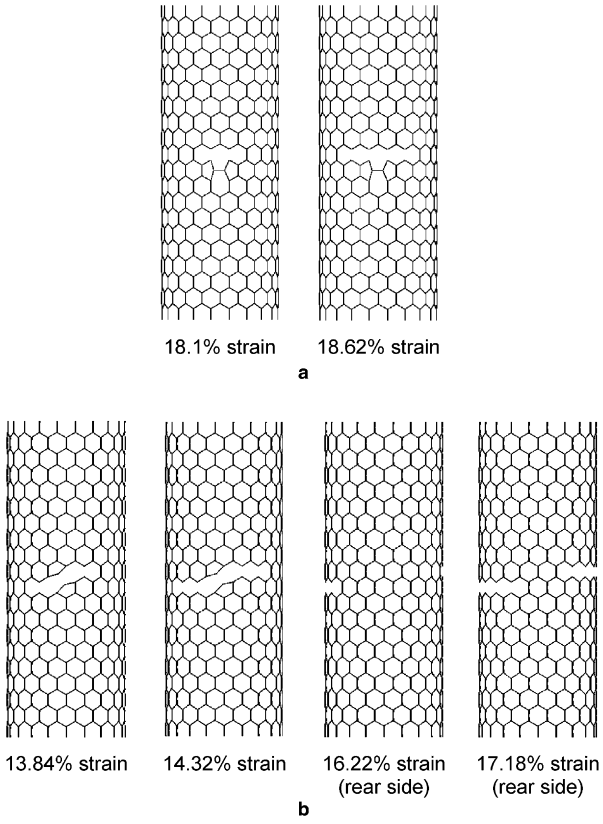

Fig. 8. Predicted fracture evolution in the zigzag (20, 0) tube containing a SW defect: (a) type I defect and (b) type II defect.

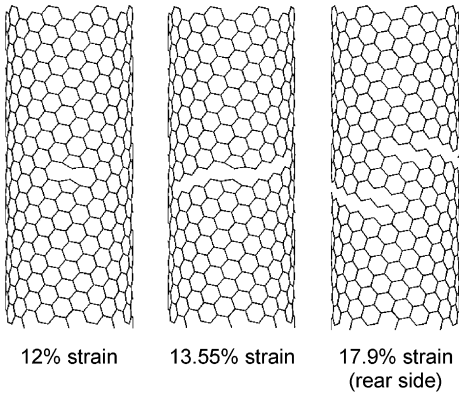

Fig. 9. Predicted fracture evolution in the chiral (16, 8) tube containing a SW defect.

6. Conclusions

In the present paper, a study was accomplished on the effect of SW defect on the tensile behavior and fracture of SWCNTs. It was found that the SW defect serves as nucleation site for fracture. Its effect on the tensile behavior of SWCNTs concerns the failure stress and failure strain and depends solely on nanotube chirality. In armchair SWCNTs, there is a significant reduction in failure stress and failure strain ranging from 18% to 25% and from 30% to 41.4%, respectively. On the other hand, in zigzag SWCNTs, the SW defect formed by the 90° rotation of a longitudinal bond does no affect their tensile behavior at all, while the defect formed by the 90° rotation of a diagonal bond reduces the failure stress and failure strain of the nanotubes by about 3% and 15%, respectively. The effect of a SW defect in chiral SWCNTs is between those of the armchair and zigzag SWCNTs according to the chiral angle. For the SW-defected (16, 8) tube considered in this work, a 15.18% reduction was predicted in the failure stress and a 32.4% in failure strain. The stiffness of the SWCNTs was not affected by the presence of SW defects. The nanotube size was found to play a minimal role on the tensile behavior of SW-defected SWCNTs; only in cases of small nanotube diameters, where the fraction of defect area to the nanotube area is high, was a larger decrease in the failure stress predicted.

Additionally to the fulfillment of the basic scope described in the previous paragraph, this paper intends also to give support to the belief that continuum mechanics methods combined to the appropriate physics can be an efficient computational tool for modeling the structure of CNTs and predicting their mechanical behavior. The PFM used to accomplish the current study treats CNTs as space-frame structures in order to enable use of finite elements for modeling their response to mechanical loading. The FE method has lent the PFM the ability to model nanotube systems with a very large number of atoms subjected to complex mechanical loading conditions in small CPU times. For example, the analysis of the (18, 18) tube (1200 atoms, 120 load steps) took about 120 s on a Pentium® 4 CPU 3.20 GHz, 1.0 GB RAM personal computer. This ability is the main advantage of atomistic-based continuum mechanics approaches over the classical atomistic modeling approaches, such as MD simulations.

The modified Morse interatomic potential used to describe the nonlinear force-field of the C–C bonds, may not be appropriate for describing fracture evolution, since it does not take into account many-body interactions as well as reconfiguration of bonds, but gives correct predictions for the fracture initiation and the behavior of the nanotube prior to fracture. Besides, the specific potential has been extensively used in the literature for predicting the mechanical properties and behavior of CNTs with success. Nevertheless, it is in the authors' interests to incorporate many-body potentials in the PFM and compare their performance in various cases against the pairwise modified Morse potential.

References

[1] Ebbesen TW, Takada T. Topological and sp^3 defect structures in nanotubes. Carbon 1995;33(7):937–78.
[2] Mielke SL, Troya D, Zhang S, Li J-L, Xiao S, Car R, et al. The role of vacancy defects and holes in the fracture of carbon nanotubes. Chem Phys Lett 2004;390:413–20.
[3] Yao Z, Postma HWC, Balents L, Dekker C. Carbon nanotube intramolecular junctions. Nature (London) 1999;402:273–6.

[4] Stone AJ, Wales DJ. Theoretical studies of icosahedral C_{60} and some related species. Chem Phys Lett 1986;128(5–6):501–3.
[5] Belytschko T, Xiao SP, Schatz GC, Ruoff RS. Atomistic simulations of nanotube fracture. Phys Rev B 2004;65:235430-1.
[6] Troya D, Mielke SL, Schatz GC. Carbon nanotube-fracture-differences between quantum mechanical mechanisms and those of empirical potentials. Chem Phys Lett 2003;382:133–41.
[7] Yakobson BI. Mechanical relaxation and "intramolecular plasticity" in carbon nanotubes. Appl Phys Lett 1998;72:918–20.
[8] Chandra N, Namilae S, Shet C. Local elastic properties of carbon nanotubes in the presence of Stone–Wales defects. Phys Rev B 2004;69:094101-1.
[9] Tserpes KI, Papanikos P. Finite element modeling of single-walled carbon nanotubes. Compos Pt B 2005;36:468–77.
[10] Tserpes KI, Papanikos P, Tsirkas S. A progressive fracture model for carbon nanotubes. Compos Pt B; in press.
[11] Brenner DW. Empirical potential for hydrocarbons for use in simulating the chemical vapor deposition of diamond films. Phys Rev B 1990;42:9458.
[12] Xiao JR, Gama BA, Gillespie Jr JW. An analytical molecular structural mechanics model for the mechanical properties of carbon nanotubes. Int J Solids Struct 2005;42:3075–92.
[13] Sun X, Zhao W. Prediction of stiffness and strength of single-walled carbon canotubes by molecular-mechanics based finite element approach. Mater Sci Eng 2005;390:366–71.
[14] Nardelli BI, Yakobson BI, Bernholc J. Mechanism of strain release in carbon nanotubes. Phys Rev B 1998;57:R4277.
[15] Zhao Q, Nardelli MB, Bernholc J. Ultimate strength of carbon nanotubes: a theoretical study. Phys Rev B 2002;65:144105.
[16] Zhang P, Lammert PE, Crespi VH. Plastic deformations of carbon nanotubes. Phys Rev B 1998;81:5346–9.